

Response to a comment on “Thermal infrared observations of a western United States biomass burning aerosol plume”

Blake T. Sorenson¹, Jianglong Zhang², Jeffrey S. Reid³

¹National Research Council, Monterey, CA 93943

²Department of Atmospheric Sciences, University of North Dakota, Grand Forks, ND, 58202

³Marine Meteorology Division, U. S. Naval Research Laboratory, Monterey, CA 93943

1. Introduction

In Sorenson et al (2024), hereafter “S24”, we reported on apparent aerosol signals in thermal infrared (TIR) imagery during a period of thick smoke plumes as observed from satellite data including the Moderate Resolution Imaging Spectroradiometer (MODIS), the Visible Infrared Imaging Radiometer Suite (VIIRS), Cloud and the Earth’s Radiant Energy System (CERES), Cross-track Infrared Sounder (CrIS), and the Geostationary Operational Environmental Satellite 17 (GOES-17). Often, smoke particles are of such a size that they are neglected for the mid-wave infrared and thermal infrared bands ($d_p < 1 \mu\text{m}$; or the size parameter < 0.3 for $\lambda = 10 \mu\text{m}$ and nearing the Rayleigh regime). Nevertheless, observers of western meteorological geostationary satellite loops often notice spatial correlation between smoke and infrared signals, and S24 took the opportunity of favorable satellite overpasses to investigate the case of the 2021 Dixie fire. S24’s conclusions noted a) the smoke’s infrared effect significantly offsets its shortwave forcing (e.g., Fig. 1); b) much of this offset is not necessarily due to the plume’s constituents of smoke particles and water vapor but there is strong evidence of surface cooling being the dominant factor in an infrared signature; and c) this is a single case study and other analyses are necessary. In this comment regarding our initial paper (with the comment hereafter referred to as F25), our assumptions and findings were questioned as misleading. However, we have been quite transparent in our analysis and as we show here the science topic is far more complex than F25 supposes. We are pleased that S24 is having the desired effect of spurring discussion on this important topic and will hopefully lead to follow-on studies.

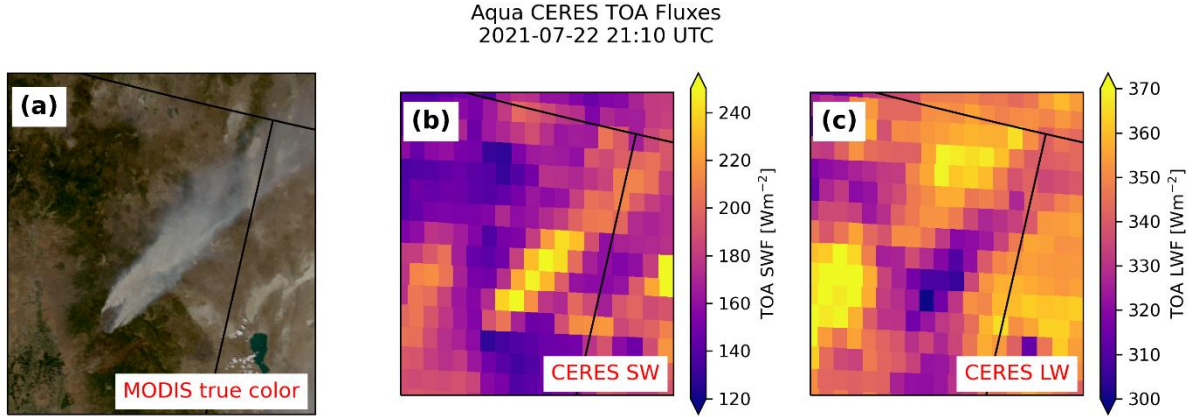


Figure 1. (a) Aqua MODIS true color imagery, (b) Aqua CERES top-of-atmosphere (TOA) shortwave flux (SW), and (c) Aqua Ceres TOA longwave flux (LW) observations in the Dixie Fire area of northeastern California and northwestern Nevada at 21:10 UTC on 22 July 2021. Note the opposite signs in changes in SW and LW flux over the plume.

F25 presented data from several dates during the Dixie Fire, arguing that the source of the observed TIR cooling signals was actually the interception of terrestrial longwave emissions by large particles, not the shadowing of the surface by fine-mode smoke particles. F25 argued that the existence of TIR cooling signals in the Dixie Fire plume at night proves that the cooling was not caused by shadowing, but by the interception of terrestrial longwave emission by large particles. F25 also argued that the TIR cooling rates in smoke plumes reported by S24 are physically unreasonable for surface cooling under shadowed conditions alone. This response addresses the critiques and evidence presented in F25 and seeks to further investigate the sources of TIR cooling signatures observed within dense smoke plumes. This response is organized as follows: in Section 2, we investigate TIR cooling signals from the Dixie Fire in several cases identified by S24 and F25 and determine the likely sources of the TIR cooling signals; in Section 3, we test our hypothesis of observable TIR cooling beneath fine-mode smoke particles by analyzing a dense fine-mode smoke event in the Northern Plains region on 29 June 2015; and in Section 4, we study the thermal response time of the Earth's surface under suddenly and significantly shadowed conditions during the 2024 total solar eclipse. We included our overall responses in the summary section.

2. Analysis of additional Dixie Fire cases

In this section, we first analyze the Dixie Fire plume signatures on 20 – 21 July 2021, which was partially analyzed in S24. Then, we analyze the Dixie Fire plume on 22 July 2021, which was the main case analyzed in S24. Finally, we analyze data for the Dixie Fire plume on 5 August 2021, a date analyzed by F25 containing strong pyroCb activity not included in the S24 analysis.

2.1 Dixie Fire on 2021/07/20 – 2021/07/21

The Aqua MODIS true-color imagery at 21:25 UTC on 20 July 2021 (Fig. 2a) shows a plume of dense biomass burning (BB) smoke extending from the Dixie Fire to the northeast in northeastern California. As the wavelength increases from the visible (Fig. 2b) to the shortwave infrared (SWIR) (Fig. 2e), the plume signature becomes significantly less pronounced. Faint plume signatures are found in the 1.24 μm data (Fig. 2d), but surface features are clearly visible through most of the smoke plume region in the 2.13 μm imagery (Fig. 2e). For example, Eagle Lake, located northeast of the Dixie Fire, is clearly visible in the 2.13 μm imagery despite being completely obscured by smoke in the visible imagery. This shows that the optical depth of the smoke in these areas decreases significantly from the visible to the SWIR wavelengths, implying that the smoke in those areas has a large Angstrom exponent and, therefore, the smoke was likely dominated by fine-mode particles. The level of contrast between surface features as viewed from satellite imagers is related to the optical depth, with lower contrast being related to higher optical depth (Hoekzema et al., 2010; Thorpe, 1979); thus, the high contrast of surface features visible in the SWIR imagery of the Dixie Fire plume implies a very low optical depth at that wavelength. It is also worth noting that the Dark Target MODIS over-land aerosol optical depth (AOD) algorithm uses 2.1 μm reflectance to quantify surface reflectance beneath fine-mode aerosol plumes, which is possible because of the very low optical depth of fine-mode aerosols, such as biomass burning smoke, at 2.1 μm (Kaufman et al., 1997; Remer et al., 2005). The Aqua MODIS TIR brightness temperatures (BTs) (Fig. 2f) show strong TIR cooling extending far downwind of the Dixie Fire, in regions with little-to-no SWIR plume signatures. Composite reflectivity fields were analyzed across the Dixie Fire plume region from three nearby WSR-88D NEXRAD radars: the Medford, OR radar (KMAX), the Beale Air Force Base radar (KBBX), and the Reno, NV radar (KRGX), and the composite reflectivity fields are shown in Fig. 2g – i. KBBX and KRGX detected some radar echoes in the regions very close to the fire, but none of the three radars detected any plume signatures across the areas far downwind of the fire where there is still significant TIR cooling.

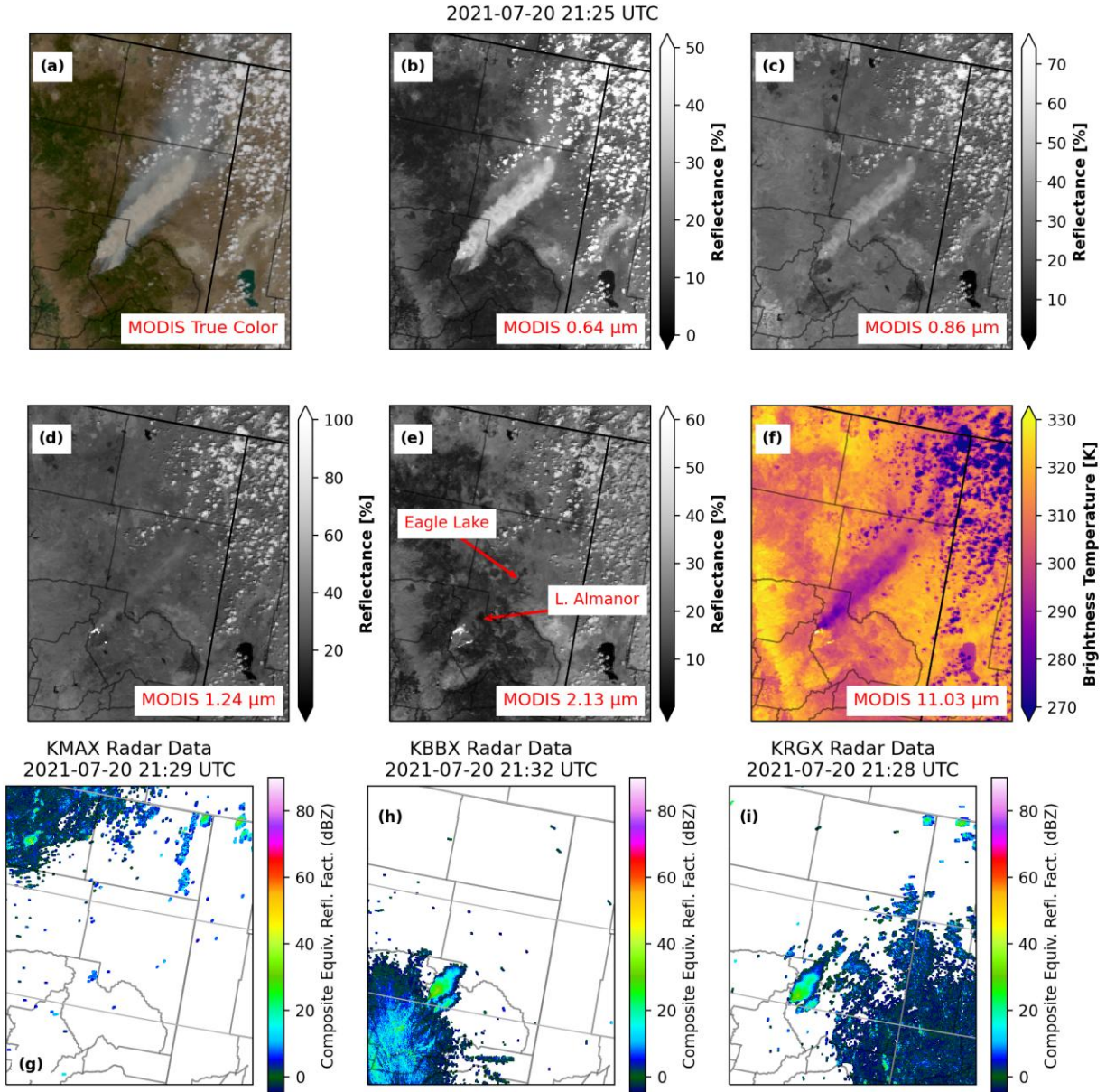


Figure 2. Aqua MODIS and NEXRAD radar observations in the Dixie Fire plume area at 21:25 UTC on 20 July 2021. Top row: Aqua MODIS (a) true color imagery, (b) 0.64 μm reflectance, and (c) 0.86 μm reflectance. Middle row: Aqua MODIS (d) 1.24 μm reflectance, (e) 2.13 μm reflectance, and (f) 11.03 μm brightness temperature. Bottom row: Composite reflectivity fields derived from (g) Medford, OR (KMAX) radar, (h) the Beale Air Force Base (KBBX) radar, and (i) the Reno, NV (KRGX) radar.

In F25, the author argues that the radar signals in the areas close to the Dixie Fire prove the existence of large particles. Thus, we analyze the MODIS data and NEXRAD radar observations in the area around and immediately downwind of the Dixie Fire in Fig. 3. Aqua MODIS true color imagery (Fig. 3a) shows very dense smoke being generated by the Dixie Fire at this time, being advected to the northeast away from the fire. The MODIS SWIR imagery (Fig. 3b), overall, show very little plume signatures, except for an area of moderate SWIR reflectance that obscures the

northwestern half of Lake Almanor. In fact, half of Lake Almanor is visible at SWIR channels, indicating the presence of fine-mode aerosols over that region. Note that even for SWIR channels, we may expect non-negligible fine mode smoke aerosol AOTs for very dense smoke regions. This may partially explain why the other half of Lake Almanor is less visible at SWIR channels. The MODIS TIR brightness temperatures (Fig. 3c) show very strong cooling in this same region. The composite reflectivity fields from KBBX and KRGX (Fig. 3e and f, respectively) show strong echoes in these areas. With the increased SWIR reflectance that obscures the surface, the significantly enhanced TIR cooling, and notable radar echoes all in the same area, it is possible that there was ash or other large pyrometeors in the plume in these locations. However, these signals are confined to the area immediately downwind of the fire. As the analysis in the previous figure showed, there are no significant SWIR signals far downwind, nor are there any notable radar echoes, but there is still strong TIR cooling in the plume region. It is also possible that Bragg scattering could play a role in the radar signatures due to the strong eddies and thermal contrast between the ambient air and the warm air above the fire (Rogers and Brown, 1997). In fact, parts of Lake Almanor, which are under thick smoke plumes in the MODIS true-color imagery and have noticeable radar echoes as shown in Fig. 3e, is visible in the $2.13\ \mu\text{m}$ imagery, indicating Bragg scattering may be partially responsible for the notable radar echoes over those regions.

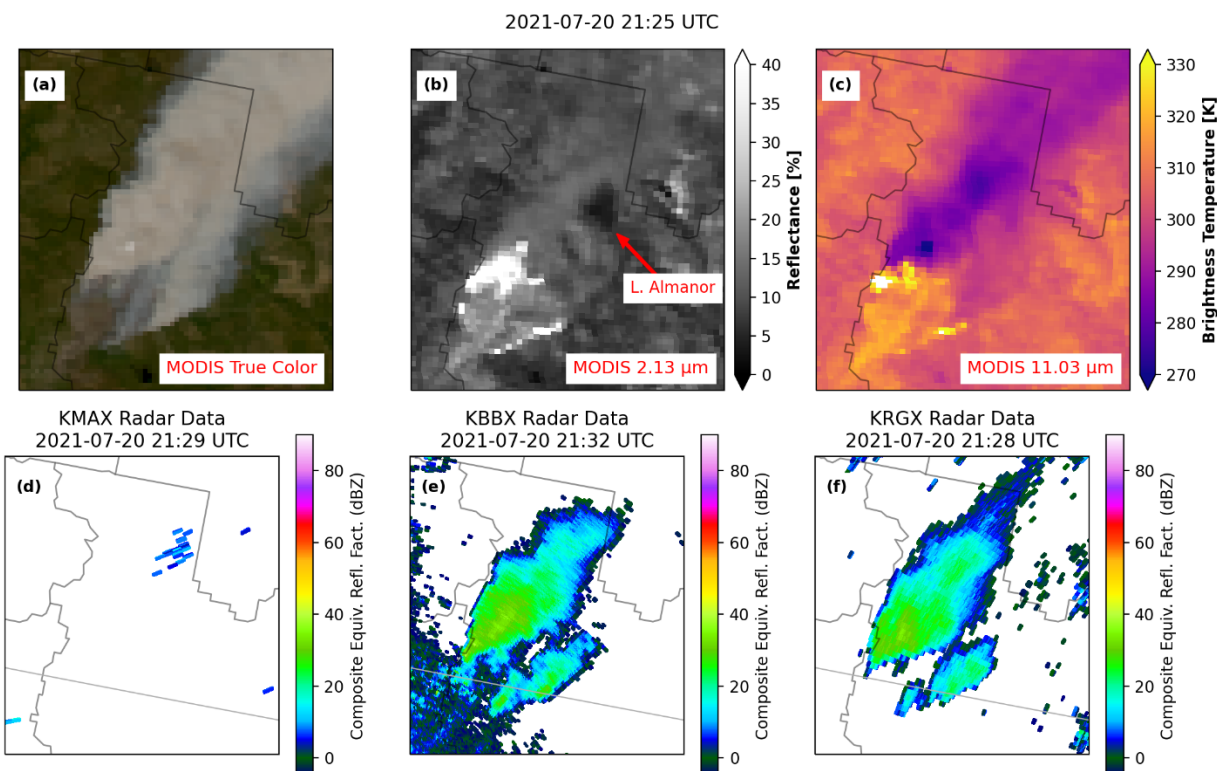


Figure 3. Comparison of Aqua MODIS data and NEXRAD composite reflectivity in the Dixie Fire area at 21:25 UTC on 20 July 2021. Top row: Aqua MODIS (a) true color imagery, (b) SWIR ($2.13\ \mu\text{m}$) reflectance, and (c) $11.03\ \mu\text{m}$ brightness temperature. Bottom row: Composite reflectivity fields derived from (d) Medford, OR (KMAX) radar, (e) the Beale Air Force Base (KBBX) radar, and (f) the Reno, NV (KRGX) radar. The dark area on the northeastern edge of the Dixie Fire in panel (b) is Lake Almanor.

As pointed out by F25, there was a small area of locally enhanced TIR cooling that is visible traveling downwind from the Dixie Fire area after sunset. This cold “bubble” is visible in the comparison of GOES-17 imagery and NEXRAD radar data at 03:30 UTC on 21 July 2021 shown in Fig. 4. A hot-spot in the Dixie Fire is visible in the GOES-17 SWIR data (Fig. 4b), suggesting the fire intensified at this time. The zone of locally enhanced TIR cooling is visible in the GOES-17 TIR data (Fig. 4c) to the northeast of this flare-up and can be seen moving to the NE in the GIF provided as a supplement. Composite reflectivity fields from the KBBX and KRGX radars, shown in Fig. 4e and f, respectively, show notable echoes in the same area as the cold “bubble”, suggesting the presence of ash in those regions. With the radar data showing echoes, and with the TIR cooling being visible at night after sunset, this case was likely driven by ash or other large pyrometeors, which was mentioned as one of the possibilities in S24. However, we cannot rule out two other possibilities at this time. The radar echoes observed near the fire may also be related to the Bragg scattering as mentioned before. It is also possible that the smoke plume is elevated and we may be observing in-smoke-shadow induced IR cooling, as 3:30 UTC is around 8:30 pm California local time.

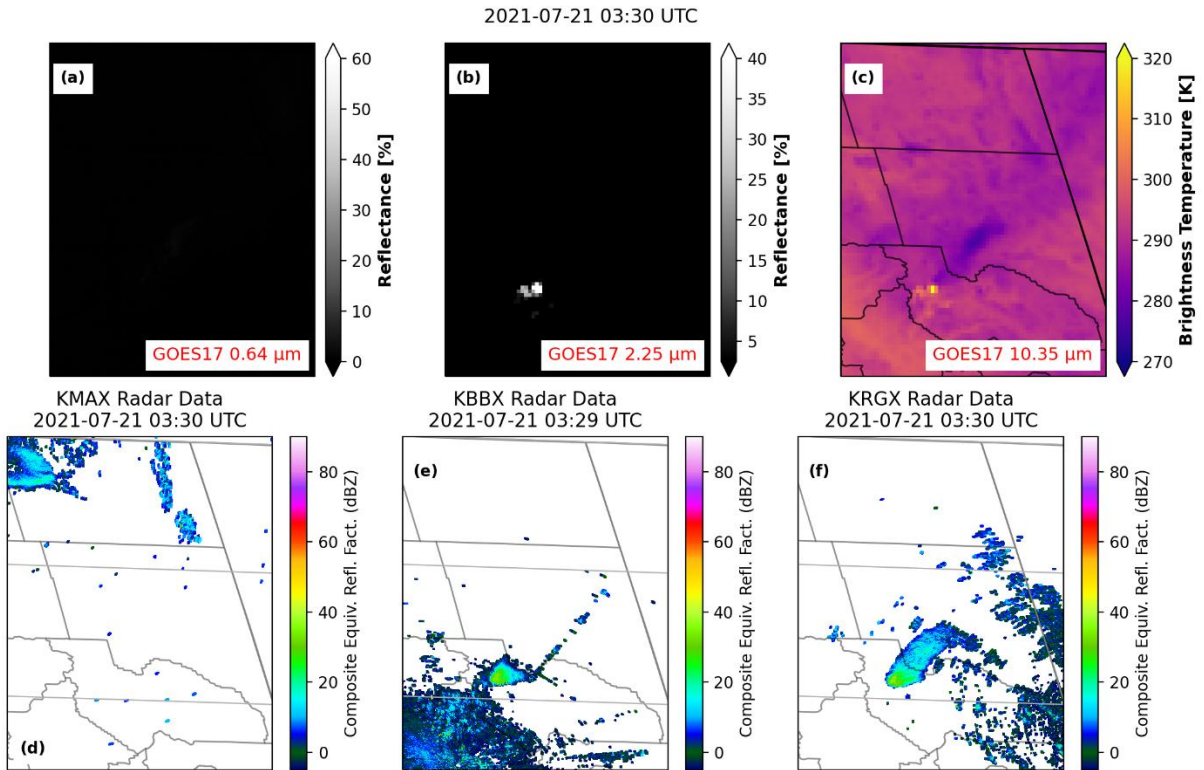


Figure 4. GOES-17 (top row) and NEXRAD (bottom row) observations in the Dixie Fire plume region of northeastern California and northwestern Nevada at 03:30 UTC on 21 July 2021. Top row: GOES-17 (a) 0.64 μm reflectance, (b) 2.25 μm reflectance, and (c) 10.35 μm brightness temperature. Bottom row: Composite reflectivity observations from (d) the Medford, OR radar (KMAX), (e) the Beale AFB radar (KBBX), and (f) the Reno, NV radar (KRGX).

However, the existence of some interception of terrestrial longwave emission by large particles in part of the plume does not prove that all of the observed TIR cooling in the Dixie Fire smoke plume

was caused by large particles. The GOES-17 visible imagery at 01:30 UTC on 21 July 2021 (Fig. 5a), just before sunset, shows widespread smoke extending far downwind of the Dixie Fire. However, the cold “bubble” found at 03:30 UTC is much smaller than this area of dense smoke, suggesting that the source of the cooling in the cold bubble was a different phenomenon than the cause of the cooling seen in the rest of the plume region. There are no significant thermal signatures in the 03:30 UTC data that cover the entire areas of smoke shown in the visible imagery at 01:30 UTC, only in one small area of that plume. Additionally, as seen in the GIF of GOES-17 and NEXRAD data through the overnight hours, no other TIR cooling signatures were observed for the rest of the night.

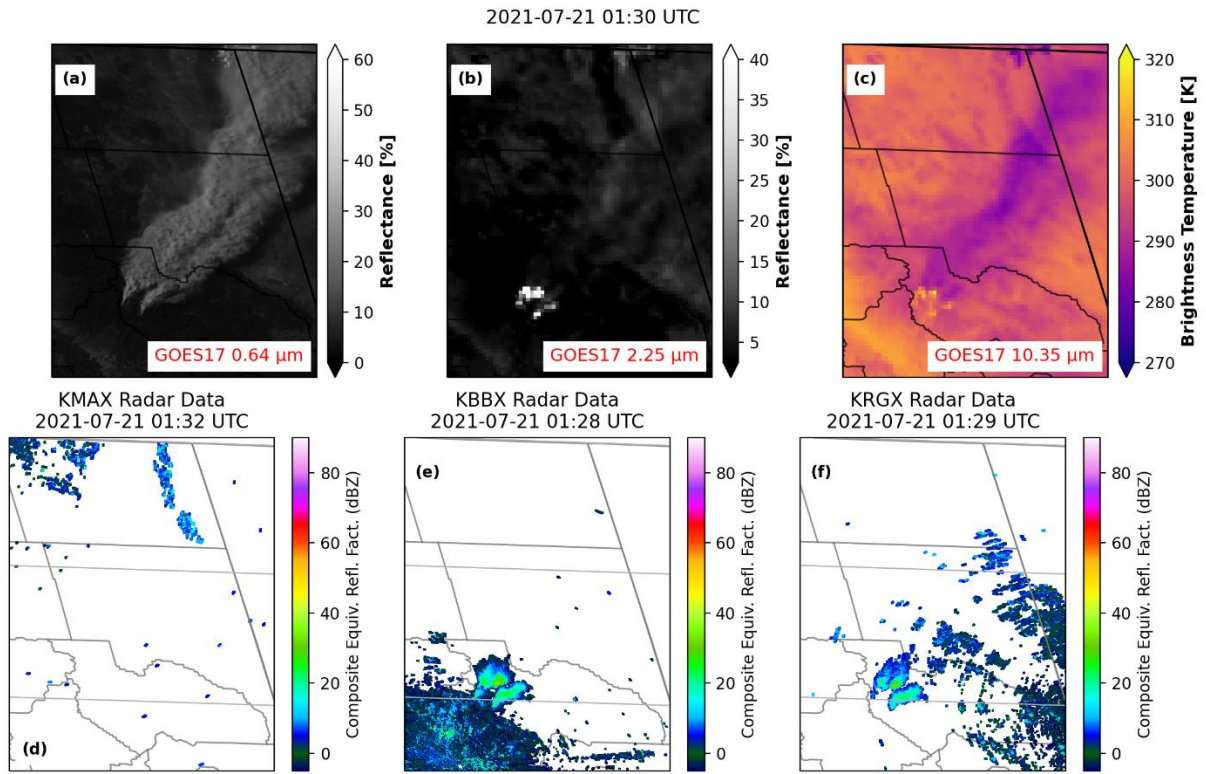


Figure 5. As in Figure 4, but showing data from 01:30 UTC on 21 July 2021.

3.2 Dixie Fire on 2021/07/22 – 2021/07/23

In this section, we analyze the Dixie Fire data on 22 July 2021. Aqua MODIS true color (Fig. 6a) and visible imagery (Fig. 6b) at 21:10 UTC show dense smoke stretching from the Dixie Fire far to the northeast, with the smoke becoming thinner downwind. As the wavelength increased from 0.64 μm to 2.13 μm , the plume signatures became significantly weaker, with some smoke being faintly visible near the fire in the 1.24 μm and being almost entirely invisible in the 2.13 μm imagery. Most notably, Eagle Lake is clearly visible in both the 1.24 μm and 2.13 μm imagery but is entirely obscured in the visible imagery. The overall lack of plume signatures in the SWIR wavelengths suggests that the optical depth of the smoke decreases significantly from the VIS to the SWIR, implying a large Angstrom exponent for the smoke particles and, therefore, fine-mode

smoke particles dominated the plume. The MODIS TIR data (Fig. 6f) show cooling across the smoky regions outlined in the visible imagery, with the strongest cooling found near the fire and weakening downwind. As with the case on 20 July 2021, we analyzed composite reflectivity fields from the three nearest NEXRAD radars (KMAX, KBBX, and KRGX), with the composite reflectivity fields shown in Fig. 6g – i. While all three radars detect some echoes immediately downwind of the fire, none of the three radars detect anything in the regions far downwind of the fire where there is still strong TIR cooling.

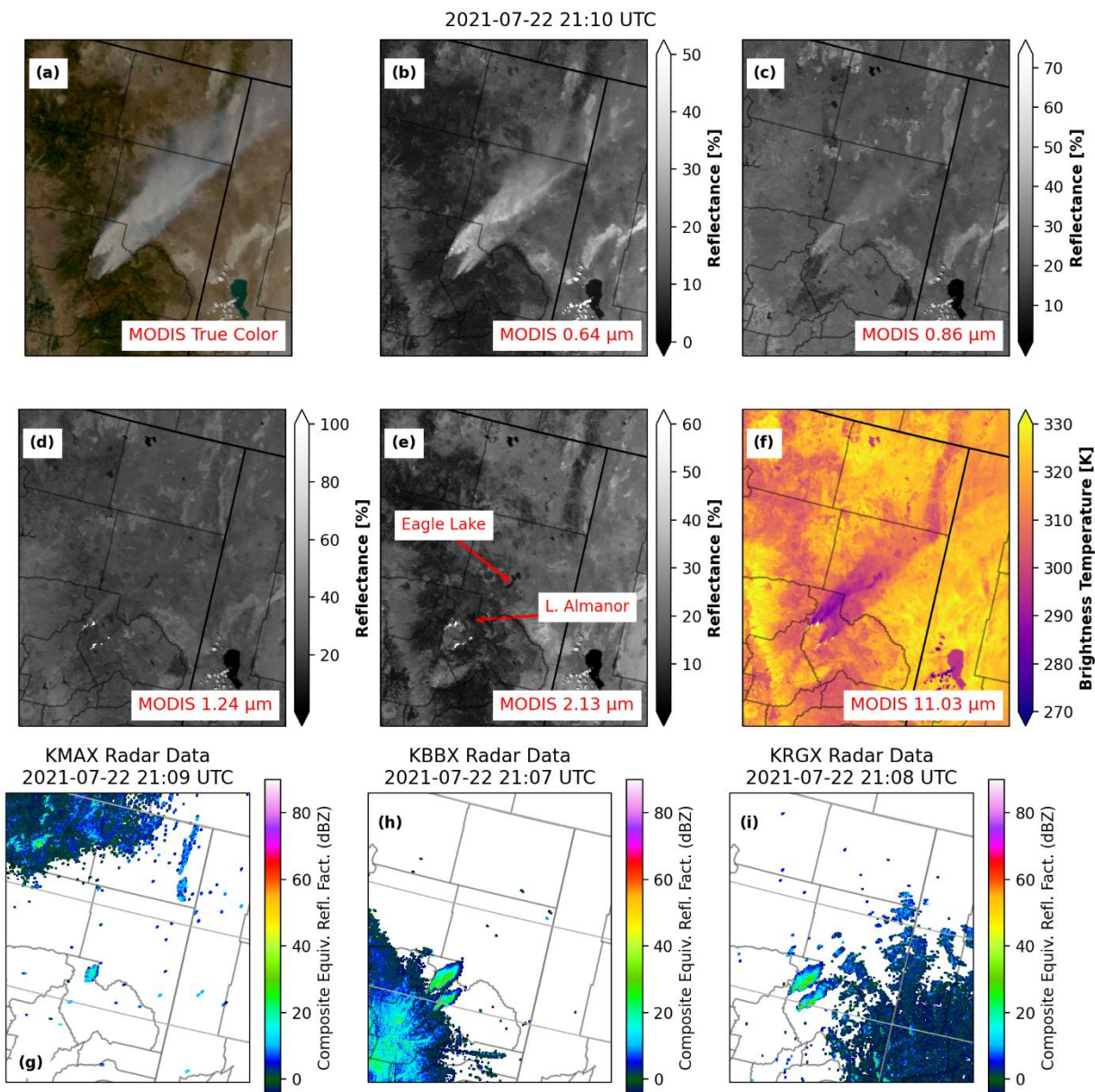


Figure 6. Aqua MODIS (a) true color imagery, (b) 0.64 μm reflectance, (c) 0.86 μm reflectance, (d) 1.24 μm reflectance, (e) 2.13 μm reflectance, and (f) 11.03 μm brightness temperature observations in the Dixie Fire region of northeastern California and northwestern Nevada at 21:10 UTC on 22 July 2021.

As with the Dixie Fire analysis on 20 July 2021, we analyze the Aqua MODIS and NEXRAD data in the region very near the fire. The Aqua MODIS true color imagery (Fig. 7a) shows plumes of dense smoke extending from the fire to the NE. The SWIR reflectance data (Fig. 7b) show clear transmission of light through much of this dense smoky area, except for some increased SWIR reflectance on the northern edge of the Dixie Fire that partially obscures Lake Almanor. The strongest TIR cooling (shown in Fig. 7c) is associated with the SWIR signals on the northern edge of Lake Almanor. Composite reflectivity fields from the three nearest radars (Fig. 7d – f) all contain echoes within the plume area just downwind of the fire, with KBBX and KRGX detecting the strongest echoes. With strong radar echoes and faint SWIR signals in the same area, it is plausible that ash and other large particles were present in the Dixie Fire in those regions, yet we could not rule out Bragg Scattering as one of the potential or even major sources of the radar echoes. This is because parts of Lake Almanor, which are within the regions of noticeable radar echoes, are observable at the 2.13 μm channel. But as with the analysis on 20 July 2021, these areas of faint SWIR reflectance and radar echoes are confined only to the area immediately downwind of the fire; the MODIS and NEXRAD data far downwind of the fire show neither increased SWIR signals nor radar echoes, suggesting that there were no large particles in those areas.

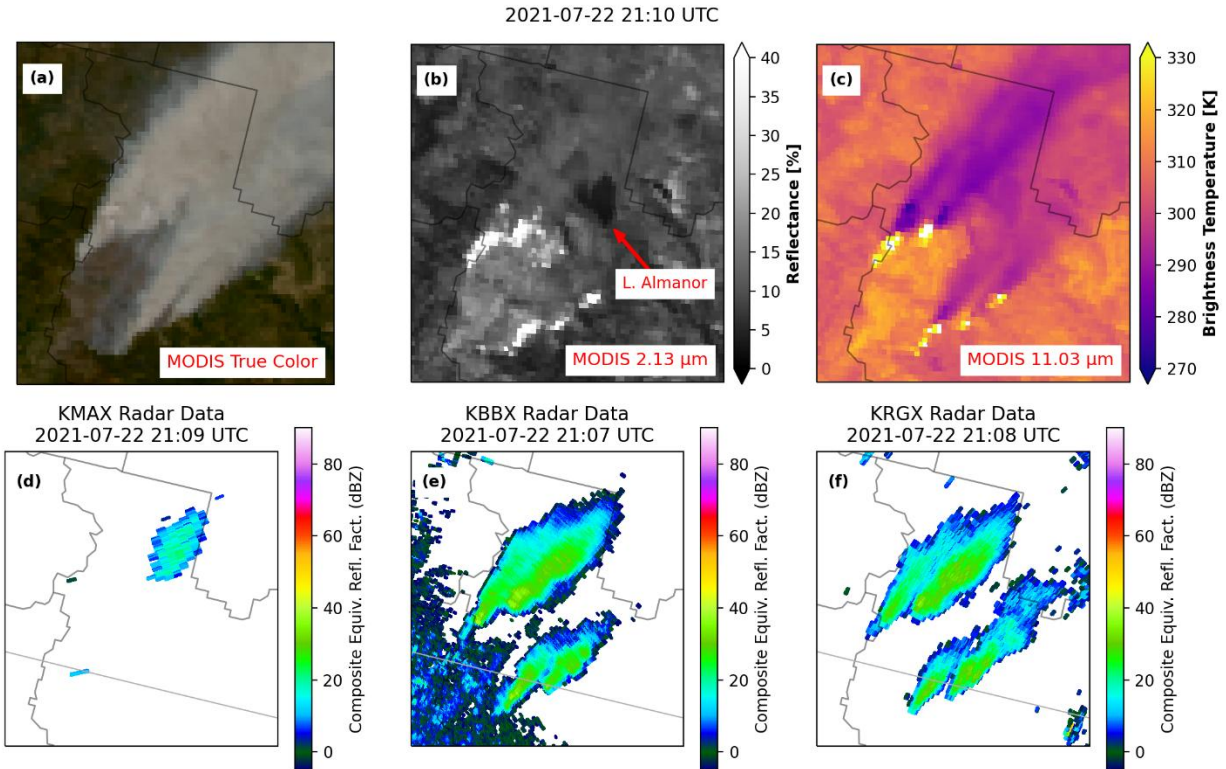


Figure 7. Comparison of Aqua MODIS data and NEXRAD composite reflectivity in the Dixie Fire area at 21:10 UTC on 22 July 2021. Top row: Aqua MODIS (a) true color imagery, (b) SWIR (2.13 μm) reflectance, and (c) 11.03 μm brightness temperature. Bottom row: Composite reflectivity fields derived from (d) Medford, OR (KMAX) radar, (e) the Beale Air Force Base (KBBX) radar, and (f) the Reno, NV (KRGX) radar. The dark area on the northeastern edge of the Dixie Fire in panel (b) is Lake Almanor.

While not shown in the figure, the Chester, CA ASOS site (O05) is located on the northwestern edge of Lake Almanor, which is visible as the dark zone in Fig. 7b just northeast of the Dixie Fire. F25 argued that the 2-m air temperatures observed by O05 and the GOES-16 TIR BTs at the location of O05 appeared decoupled during 22 July 2021, implying that GOES-16 was not detecting the surface and was instead detecting ash. We have several issues with the GOES-16 / ASOS analysis presented in the comment. First, F25 does not account for the impacts of advection and/or mixing on the 2-m air temperature measurements obtained by O05 that could have led to the 2-m air temperatures behaving differently than the surface skin temperature. Second, the GOES-16 TIR data at the latitude and longitude of the O05 location may not be sufficiently representative of the land surface conditions at that location. The Chester, CA ASOS site is located less than one kilometer from the shore of Lake Almanor. The nadir footprint size of the GOES-16 TIR channels is 2 km, and with the western US being towards the edge of the GOES-16 field of view, the size of the GOES-16 TIR channel footprint could be as large as 3-4 km. Also, by considering geolocation, parallax and point-spread error of GOES-16, it is possible that the GOES-16 TIR brightness temperature data as shown in F25 were contaminated by the surface of Lake Almanor; this could explain why the GOES-16 data taken towards its limb do not exhibit as large of temperature variations as those exhibited by the 2-m air temperature measurements. Even if GOES-16 was contaminated by large particles above O05 on 22 July 2021, this only has implications on the TIR cooling observed immediately downwind of the fire and does not affect the TIR cooling far downwind. In those regions far downwind of the fire, there is still strong TIR cooling in the MODIS data, but neither the SWIR observations nor any of the nearest three radars give any evidence of widespread large particles in the plume. Thus, we still conclude that the TIR in those areas was caused by surface shadowing.

F25 disagreed with the VIIRS nighttime analysis presented in S24, claiming that GOES-16 data showed TIR cooling signals after sunset in the very early UTC hours on 23 July 2021. F25 argued that the TIR cooling signals at the time of the VIIRS overpass could have been too faint to be differentiable from ground features in the imagery. There certainly could have been nighttime TIR cooling signals caused by large particles in the early nighttime hours (UTC) on 23 July 2021. But by 09:42 UTC on 23 July 2021, as the VIIRS day-night band (DNB) and TIR data clearly show in Fig. 8b and e, there were no smoke patterns detected in the nighttime TIR data. Surface features in high contrast are clearly discernible in the TIR data despite being totally obscured in the DNB data, showing that the smoke was transparent to infrared radiation. F25 even admits that the smoke particle size could have diminished enough by the time of the VIIRS overpass to be transparent in the IR channels, which we agree is likely the case. Possible TIR cooling from large particles earlier in the night does not disprove the fact that the smoke at 09:42 UTC was transparent in the IR.

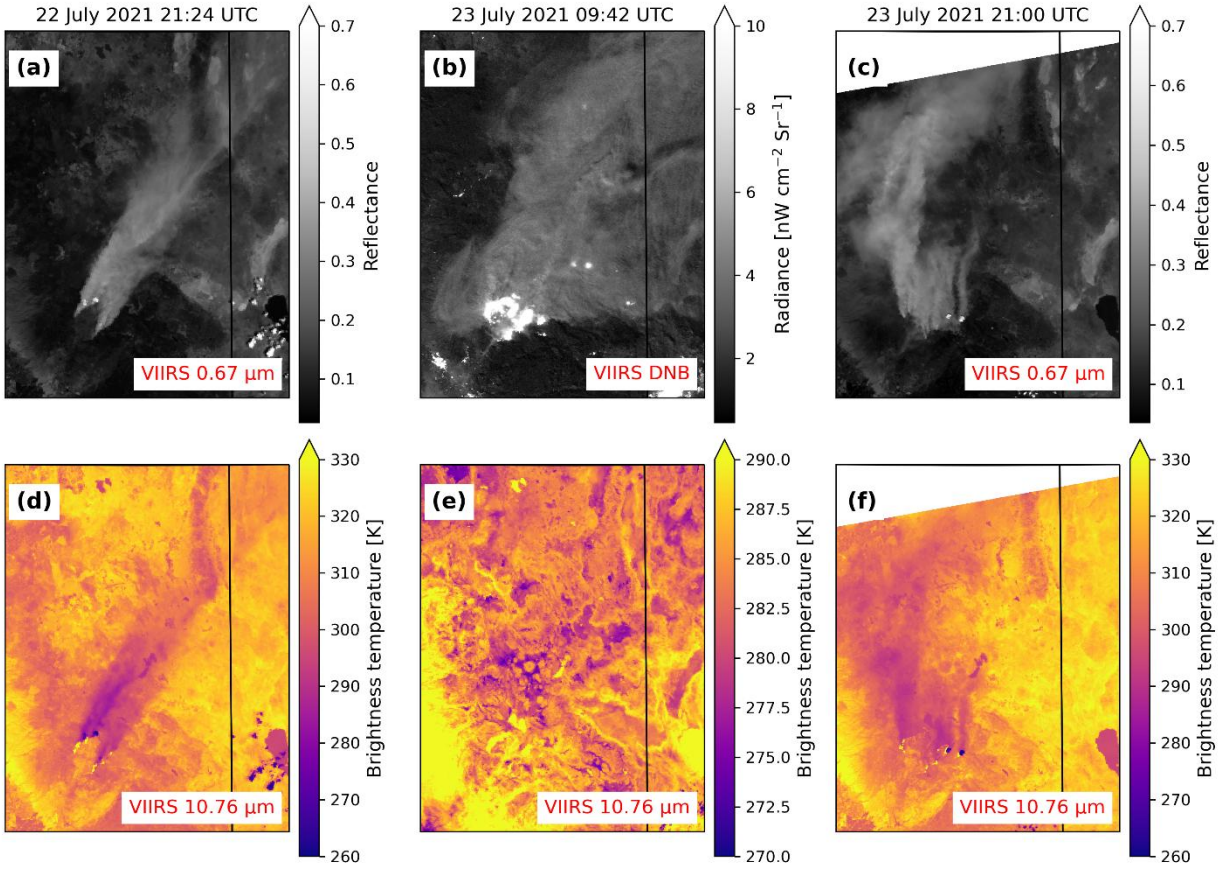


Figure 8. Suomi-NPP VIIRS (a and c) visible reflectance, (b) day-night band radiance, and (d – f) 10.76 μm brightness temperature data in the Dixie Fire plume region from (left) 21:24 UTC 22 July 2021, (middle) 09:42 UTC 23 July 2021, and (right) 21:00 UTC 23 July 2021. Figure taken from Sorenson et al (2024).

3.3 Dixie Fire on 2021/08/05

In this section, we analyze the Dixie Fire smoke plumes on 5 August 2021 brought forth by F25, when there was intense pyroCb activity. This is indeed an interesting case, and we thank F25 for bringing it to light. We first analyze GOES-17 and NEXRAD data in the pre-sunrise hours of the day. F25 correctly identified a zone of strong TIR cooling in the GOES-17 10.35 μm data associated with an intensification of the fire near that location; this zone of locally enhanced TIR cooling is visible in the GOES-17 TIR observations in Fig. 9c and in the associated GIF included as a supplement. All three of the nearest WSR-88D NEXRAD radars (Medford, Oregon (KMAX), Beale Air Force Base (KBBX), and Reno, Nevada (KRGX)) reported echoes in the same areas as the nighttime TIR cooling, as shown in the composite reflectivity fields plotted in Fig. 9d – f. With strong TIR cooling observed overnight and with all three nearby radars detecting signals in the area, we agree with F25 that the TIR cooling observed in this case was likely caused by ash and other large pyrometeors generated by a flare-up of the Dixie Fire.

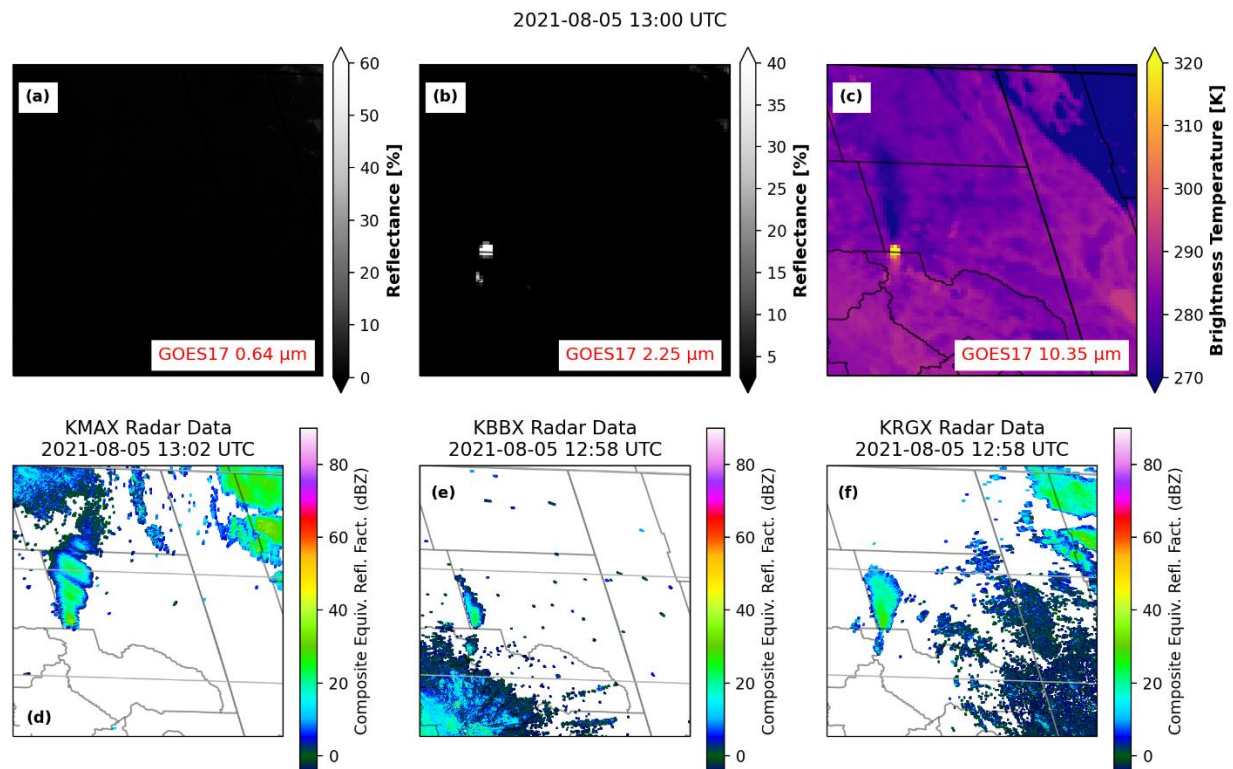


Figure 9. GOES-17 (top row) and NEXRAD (bottom row) observations in the Dixie Fire plume region of northeastern California and northwestern Nevada at 13:00 UTC on 5 August 2021. Top row: GOES-17 (a) 0.64 μm reflectance, (b) 2.25 μm reflectance, and (c) 10.35 μm brightness temperature. Bottom row: Composite reflectivity observations from (d) the Medford, OR radar (KMAX), (e) the Beale AFB radar (KBBX), and (f) the Reno, NV radar (KRGX).

Later in the day on 5 August 2021, at 21:25 UTC, both the Aqua MODIS data and GOES-17 data (Fig. 10) show two large pyroCb clouds over the Dixie Fire. The pyroCb clouds are clearly distinguishable in both the visible and the SWIR wavelengths. TIR cooling immediately downwind of the fire is very strong, and all three radars reported notable echoes in these regions. However, upon careful analysis of the visible imagery, SWIR imagery, and TIR brightness temperatures, it appears that there are two modes / sources of TIR cooling occurring at this time. Near the fire, in region with both notable radar echoes and strong SWIR reflectance signals that obscure the surface, there are very strong TIR cooling patterns. The TIR cooling observed in these regions may be due to the interception of terrestrial longwave emission by large particles. However, there is also TIR cooling in areas with neither SWIR signals nor radar echoes. For example, note that Eagle Lake is visible in both the SWIR imagery and TIR data through the smoke and between the two zones of very strong TIR cooling just downwind of the fire, but the lake is totally obscured in the visible imagery. Additionally, the Warner Mountains in northeastern California are clearly visible in the SWIR imagery and TIR brightness temperature data, though they are obscured in the visible reflectance data. None of the three closest radars detect ash echoes in the Warner Mountains or surrounding regions. Interestingly, KMAX partially detects the Warner Mountains, so KMAX is “seeing” the ground there. If there were particles large enough to be detected by radar (i.e. ash), then KMAX should have detected them. However, there are no ash echoes detected there, even

though there is a lot of visibly dense smoke over those mountains. We thus conclude that there were likely two modes of cooling occurring in this case: shadow-based cooling occurring far downwind of the fire (and in pockets near the fire), and particle-based cooling occurring in the pyroCb clouds and in other areas just downwind of the fire.

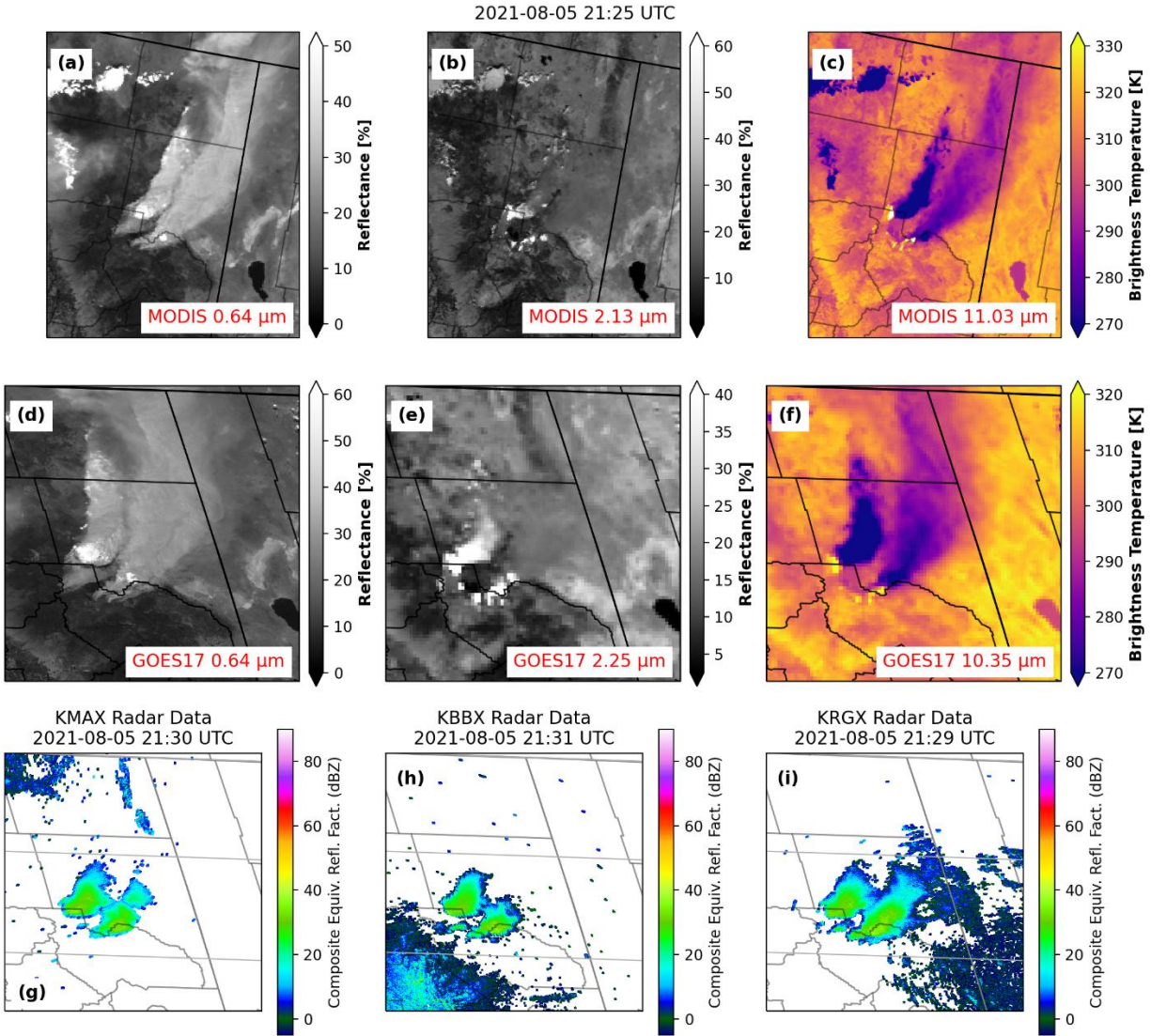


Figure 10. MODIS (Top row), GOES-17 (middle row), and NEXRAD (bottom row) observations of the Dixie Fire at 21:25 UTC on 5 August 2021. Top row: Aqua MODIS (a) 0.64 μm visible reflectance, (b) 2.13 μm reflectance, and (c) 11.03 μm brightness temperature. Middle row: GOES-17 (d) 0.64 μm visible reflectance, (e) 2.25 μm reflectance, and (f) 10.35 μm brightness temperature. Bottom row: Composite reflectivity derived from (g) the Medford, OR (KMAX) NEXRAD radar, (h), the Beale Air Force Base (KBBX) NEXRAD radar, and (i) the Reno, NV (KRGX) NEXRAD radar.

The dual polarization variables from the KBBX radar can give further insight into the composition of the Dixie Fire smoke plume near the fire. Range-Height Indicator (RHI) cross sections through the Dixie Fire plume echoes are shown in Fig. 11d – f, with the positions of the cross sections overlaid on the spatial radar images in Fig. 11a - c. The reflectivity data show a core of high

reflectivity (around 30 – 40 dBZ) immediately downwind of the fire, with the reflectivity getting weaker farther downwind. The correlation coefficient values are almost entirely below 0.6, showing the targets being detected are likely non-meteorological. Finally, the differential reflectivity (ZDR) values are near zero in the area immediately downwind of the fire, with very high (≥ 5) dBZ on the far edge of the plume echoes. These correlation coefficient and differential reflectivity patterns agree with previous radar observations in wildfire smoke plumes that other studies have attributed to ash and pine needles (see McCarthy et al., 2019 and references therein). The low ZDR in the high reflectivity core near the fire may represent ash and other debris “tumbling” in the rising air above the fire. Then, as the debris exits the rising air and falls out of the plume downwind, it “flutters down” horizontally, which could lead to the very high ZDR downwind. With the Aqua MODIS and GOES-17 SWIR data both showing increased reflectance that obscures the surface in the same areas as strong NEXRAD radar echoes, whose dual polarization variables mirror patterns others have attributed to ash and other large debris, we suspect the TIR cooling immediately downwind of the Dixie Fire could have been caused by ash and other large particles, though we cannot totally rule out Bragg scatter from affecting the observed radar echoes near the fire.

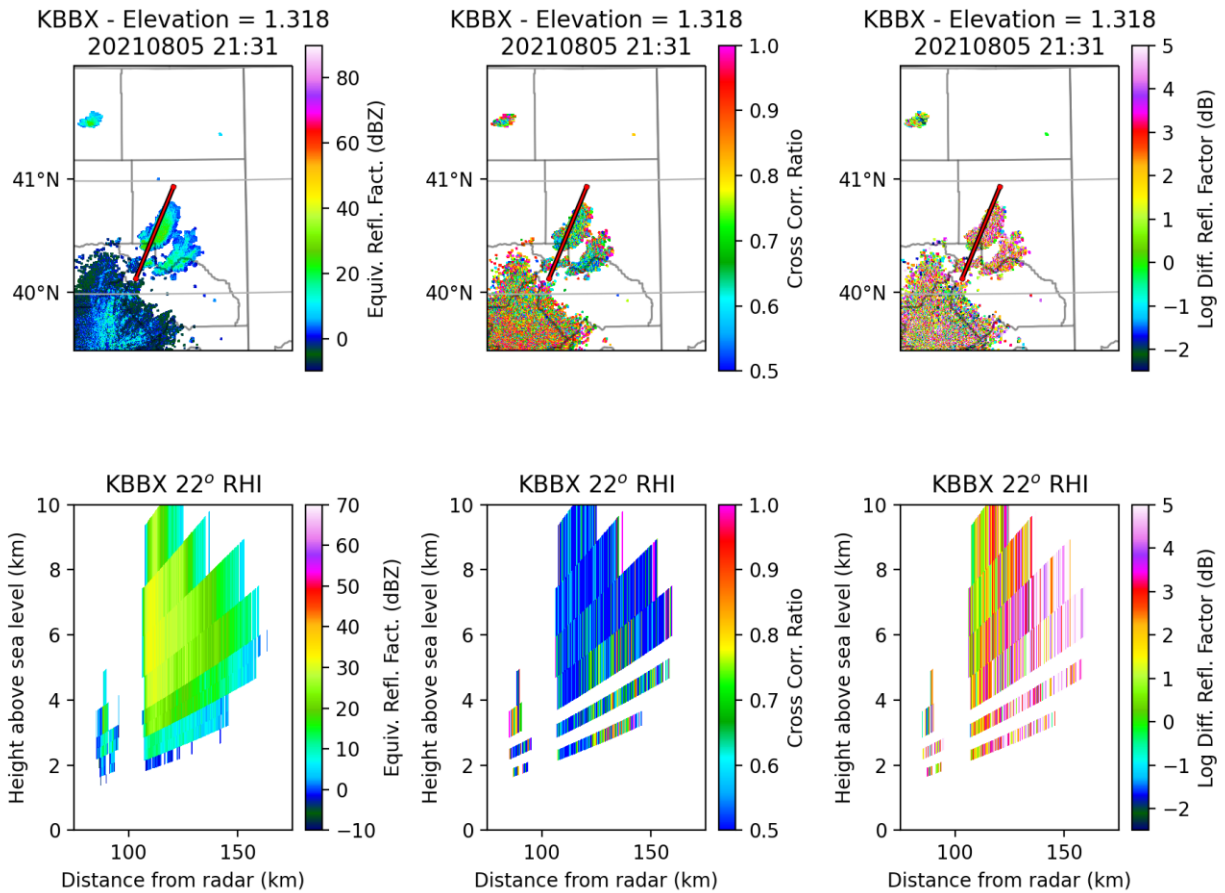


Figure 11. Observations from the Beale Air Force Base (KBBX) NEXRAD WSR-88D 10-cm weather surveillance radar of the Dixie Fire smoke plume at 21:30 UTC on 5 August 2021. Top row: Plan Position Indicator (PPI) of (a)

base reflectivity, (b) cross correlation ratio, and (c) differential reflectivity. Bottom row: Range-Height Indicator (RHI) of (a) base reflectivity, (b) cross correlation ratio, and (c) differential reflectivity taken along the 22-degree azimuth from KBBX. The red line in panels (a) through (c) show the location of the cross sections plotted in panels (d) through (f).

A few hours later, as shown in GOES-17 observations at 23:00 UTC on 5 August 2021 (Fig. 12), the pyroCb activity intensified. The regions of strong SWIR signals grew much stronger and extended very far downwind. Unlike in the Aqua MODIS and GOES-17 data at 21:25 UTC shown in Fig. 10, where the Warner Mountains were clearly visible through the smoke in both the SWIR and TIR imagery despite being obscured in the visible imagery, the Warner Mountains are no longer visible in either the SWIR or the TIR imagery at 23:00 UTC, as shown in Fig. 12b and c, respectively. With the SWIR reflectance increasing enough to totally obscure the Warner Mountains this suggests the presence of large particles (either cloud or coarse-mode smoke) in those regions. The TIR cooling also became significantly stronger, further suggesting that particle-based cooling was occurring and dominant in the plume region. However, we still cannot rule out the possibility that the obscuration of the Warner Mountains in the SWIR channels is due to non-negligible residual AOD values in the SWIR channel due to the very dense smoke in the visible imagery.

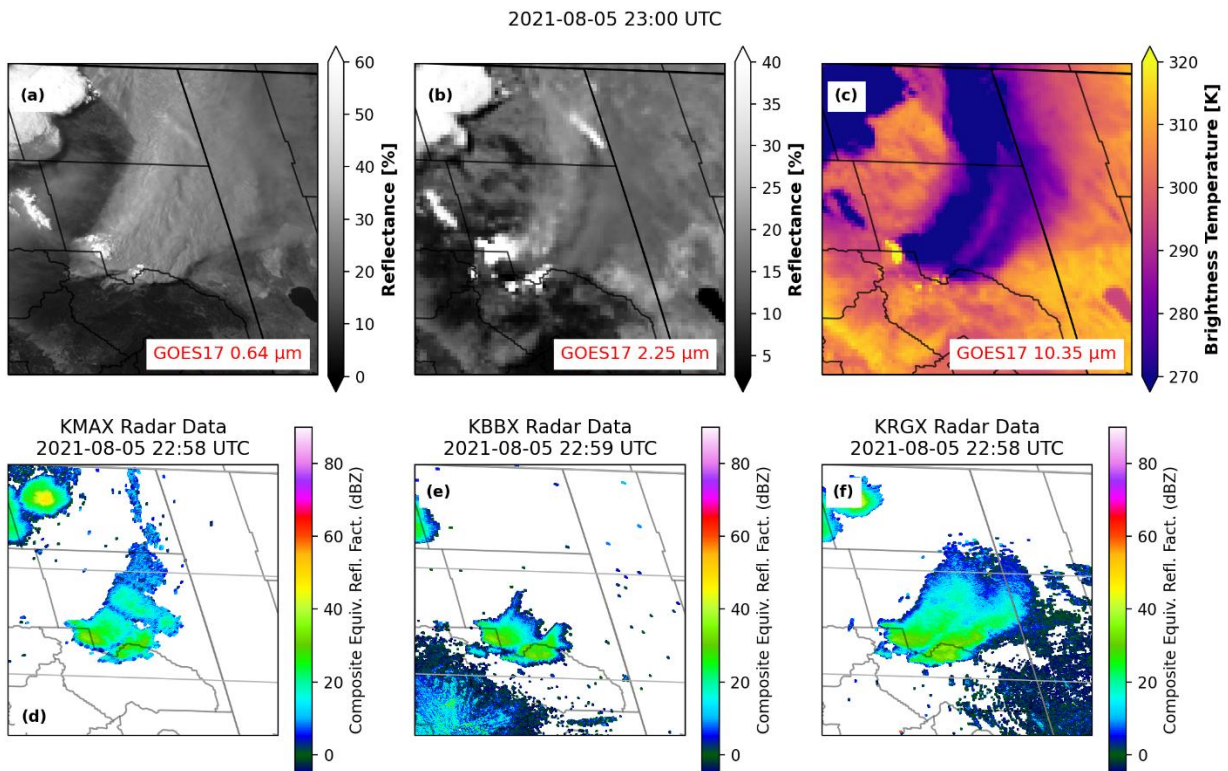


Figure 12. GOES-17 (top row) and NEXRAD (bottom row) observations in the Dixie Fire plume region of northeastern California and northwestern Nevada at 23:00 UTC on 5 August 2021. Top row: GOES-17 (a) 0.64 μm reflectance, (b) 2.25 μm reflectance, and (c) 10.35 μm brightness temperature. Bottom row: Composite reflectivity observations from (d) the Medford, OR radar (KMAX), (e) the Beale AFB radar (KBBX), and (f) the Reno, NV radar (KRGX).

As with the CERES analysis on 22 July 2021, Aqua CERES top-of-atmosphere (TOA) upwelling flux observations in the Dixie Fire plume region for the 21:25 UTC 5 August 2021 overpass (Fig. 13) show how the thermal cooling impacts the radiative effect of the plume. The increased TOA upwelling SWF in the plume region is clearly visible in Fig. 13b. The TOA upwelling LWF data, shown in Fig. 13c, reveal significant lower flux in the plume region relative to the surrounding smoke and cloud-free areas. Thus, the total radiative effect of the smoke plume is moderated by the significant reduction in TOA upwelling LWF in the plume region.

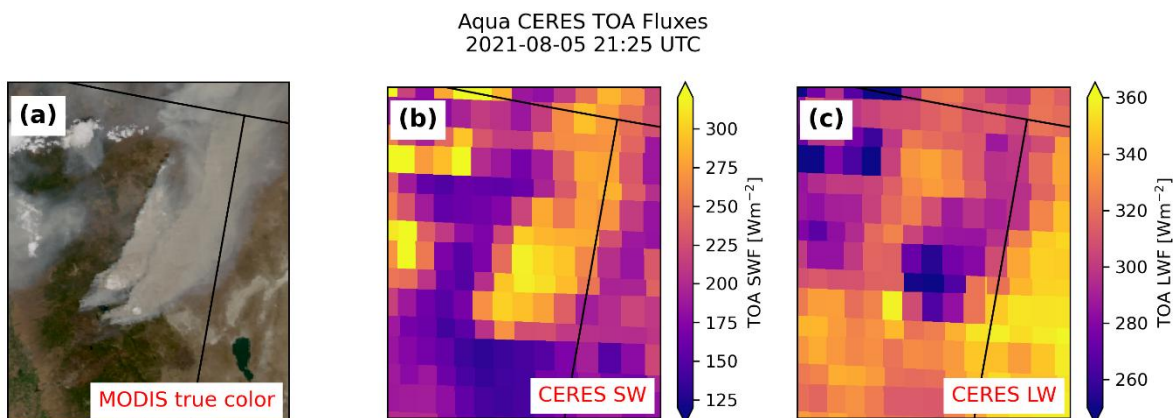


Figure 13. (a) Aqua MODIS true color imagery, (b) Aqua CERES TOA shortwave flux (SW), and (c) Aqua Ceres TOA longwave flux (LW) observations in the Dixie Fire area of northeastern California and northwestern Nevada at 21:25 UTC on 5 August 2021. Note the opposite signs in SW and LW flux over the plume.

3. Hypothesis test of observable surface shadow cooling in smoke

In the previous section, we analyzed TIR cooling signals observed in the Dixie Fire smoke plume, identifying instances of both shadow-based TIR cooling and particle-based TIR cooling. To further test our hypothesis that cooling of the surface beneath plumes of fine-mode smoke particles can be detected by thermal infrared satellite observations, we analyze a smoke event in the Northern Plains from 29 June 2015. This smoke event was caused by strong wildfires in Saskatchewan, with the lofted smoke being advected down over the Northern Plains areas of North Dakota, South Dakota, and Minnesota. Previous studies of this smoke event have already reported significant near-surface air temperature cooling in both observations and models (Carson-Marquis et al., 2021; Zhang et al., 2016). Additionally, there is an Aerosol Robotic Network (AERONET) site in Grand Forks, ND, giving us more information about the spectral optical depths and fine mode fraction of the smoke.

Figure 14 shows Aqua MODIS observations of the smoke plume in the Northern Plains region on 29 June 2015. The smoke is clearly visible in the true color (Fig. 14a) and visible reflectance data, but the smoke signals entirely disappear as the wavelength increases to $2.13 \mu\text{m}$ (Fig. 14e). There was strong TIR cooling in the smoky region as detected by the Aqua MODIS TIR data shown in Fig. 14f. As with some of the Dixie Fire cases, the lack of smoke plume signatures in the longer wavelengths (SWIR) show that the optical depth of the smoke plume decreases significantly from

the visible to the SWIR wavelengths, implying a large Angstrom exponent and fine-mode particle sizes.

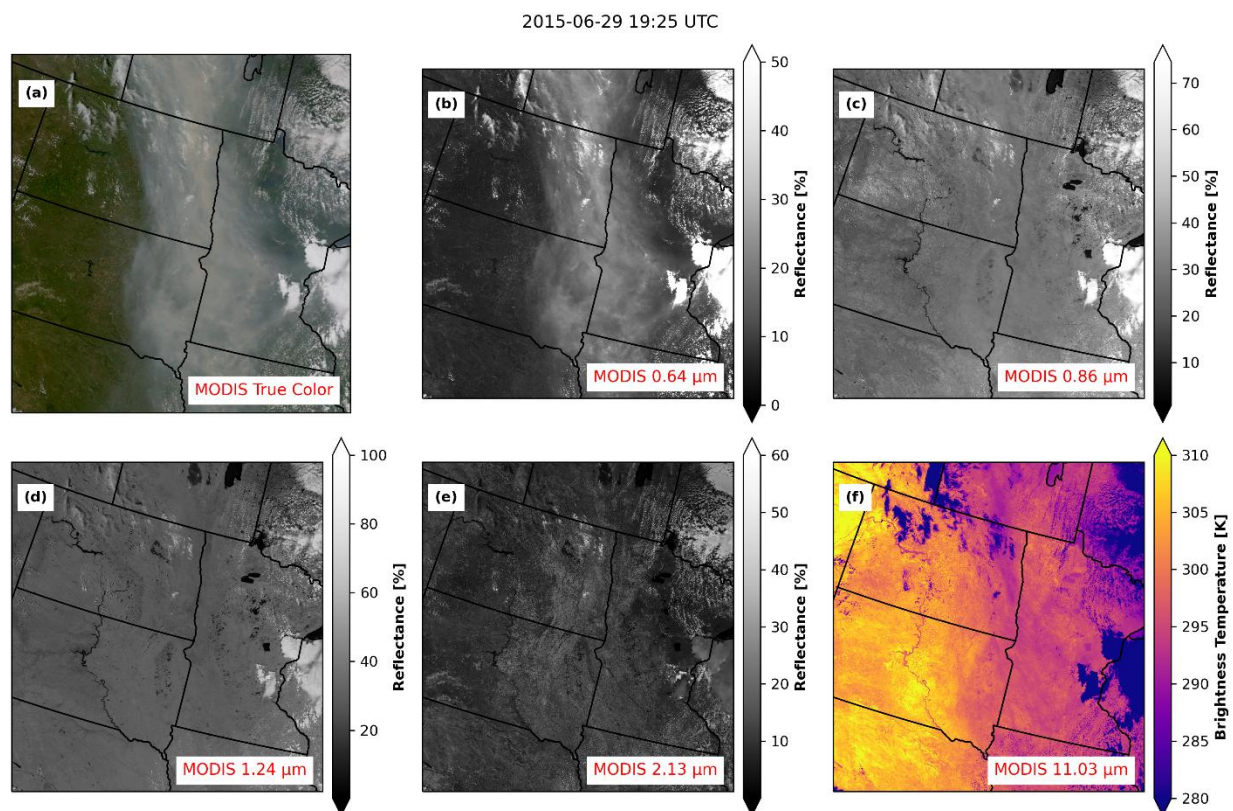


Figure 14. Aqua MODIS (a) true color imagery, (b) 0.64 μm reflectance, (c) 0.86 μm reflectance, (d) 1.24 μm reflectance, (e) 2.13 μm reflectance, and (f) 11.03 μm brightness temperature observations during the Canadian smoke event in North Dakota, South Dakota, and Minnesota at 19:25 UTC on 29 June 2015.

To verify the particle size regime of the plume inferred from MODIS, we analyze AERONET data collected from Grand Forks, ND during the smoke event. The AERONET spectral AODs and fine mode fraction are plotted as the left and right panels of Fig. 15. The AERONET AOD data exhibit very high visible AOD of 4.6. The fine-mode fraction reported by the instrument was 0.99, showing the plume consisted of entirely fine-mode smoke aerosol particles. While the plume was fine-mode, there was a non-negligible SWIR AOD of 0.35 reported by AERONET. This is not surprising, as in very high AOD scenarios, there can be some residual signal in the SWIR wavelengths; the existence of some SWIR AOD signal does not prove the presence of coarse-mode particles. Even though the smoke particles were in the fine-mode, there was still strong TIR cooling observed by MODIS, suggesting that the cooling observed by MODIS was driven not by the interception of terrestrial longwave emission by large particles, but rather by surface shadowing beneath the fine-mode smoke particles.

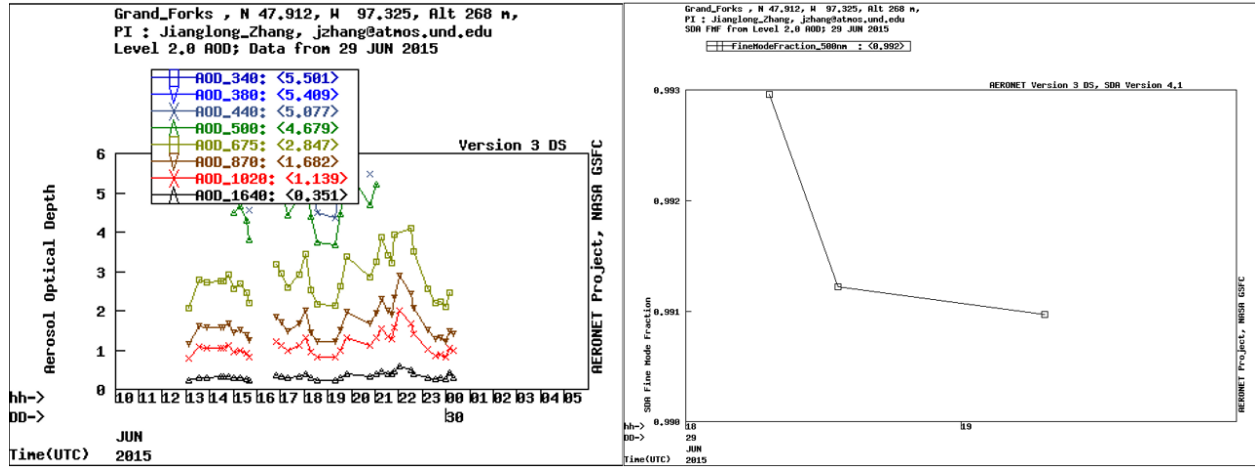


Figure 15. Left: Multispectral aerosol optical depth (AOD) observations from the AERONET site in Grand Forks, ND on 29 June 2015. Right: Fine-mode fraction derived from the AERONET observations. Figures obtained from the AERONET data viewer webpage on the NASA Goddard Space Flight Center (GSFC) website at <https://aeronet.gsfc.nasa.gov/>.

A closer look at the MODIS data in northeastern North Dakota (shown in Fig. 16) shows that some of the smoke was located over some clouds. If the TIR cooling observed within the smoky region was caused by the interception of terrestrial longwave emission by the smoke particles themselves, we would expect the cloud-free smoky regions to appear as cold as (or colder than) the cloudy areas because the smoke particles were higher in the atmosphere. However, the Aqua MODIS TIR BTs (Fig. 16f) in the clouds within the smoky regions are significantly lower than the nearby cloud-free smoky areas. This shows that the TIR cooling observed in this plume was not driven by the particles themselves, but by shadowing of the surface that was visible in the TIR wavelengths through the smoke. This case supports the hypothesis presented in S24 that surface shadowing by dense plumes of fine-mode biomass burning smoke causes strong surface cooling that can then be observed from infrared channels on satellite-based remote sensing instruments.

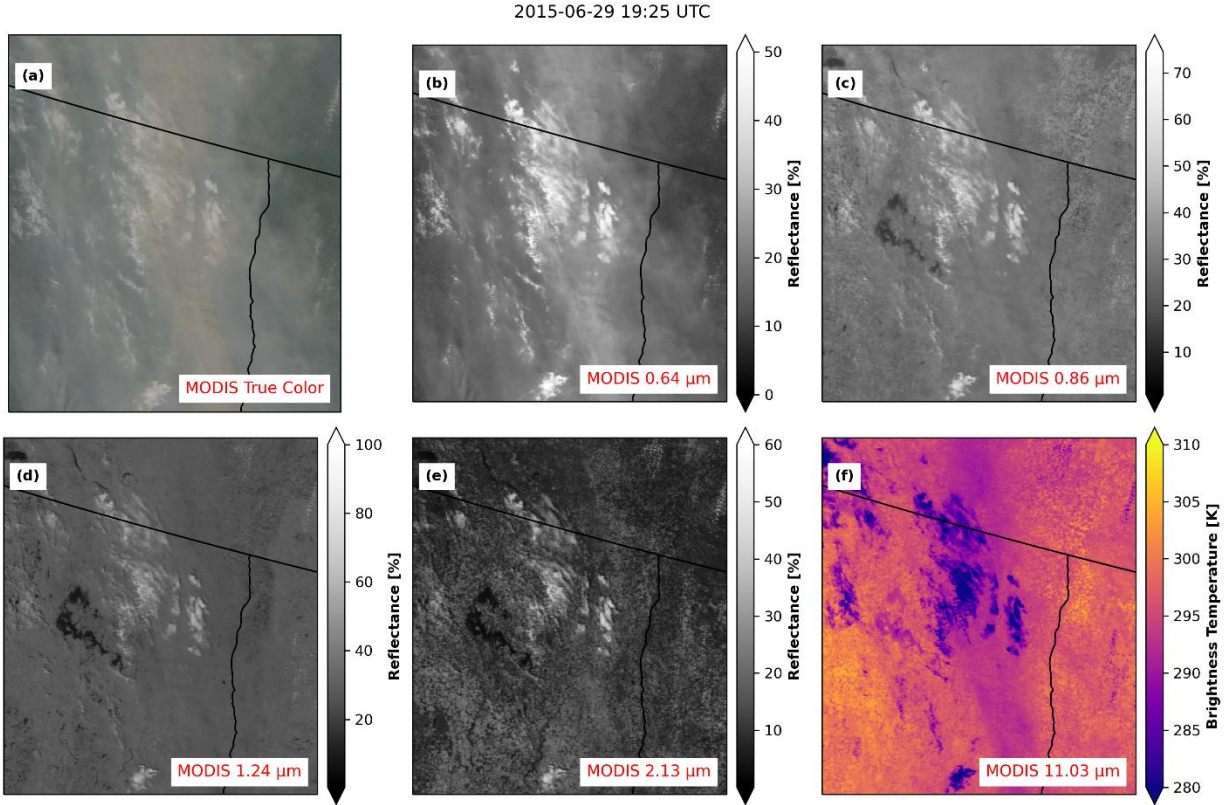


Figure 16. As in Fig. 14, but zoomed in on northeastern North Dakota.

As with the previous cases, Aqua CERES flux observations in the smoke plume region reveal how the TOA radiative effect of the smoke is moderated by the TIR cooling. The Aqua CERES fluxes observed during the 29 June 2015 smoke event in the Northern Plains (Fig. 17) show increased SWF in the smoky region. The LWF observations also show a clear reduction in TOA LWF in the smoky region, mirroring the cooling pattern found in the MODIS TIR imagery. This case also shows that reductions in LWF in smoky regions moderate the total TOA radiative impacts of smoke plumes.

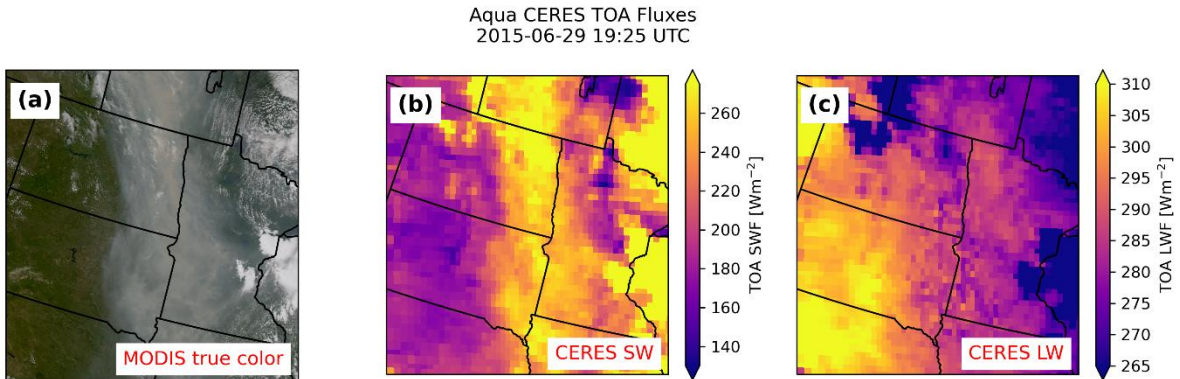


Figure 17. (a) Aqua MODIS true color imagery, (b) Aqua CERES TOA shortwave flux (SW), and (c) Aqua Ceres TOA longwave flux (LW) observations in the Canadian smoke event over North Dakota, South Dakota, and Minnesota on 29 June 2015. Note the opposite signs in SW and LW flux over the plume.

4. Thermal response time

In F25, the author critiques the smoke shadowing hypothesis and analyses presented in S24, dismissing them while stating: “simply considering Earth-surface radiative inertia, it would seem physically implausible for skin temperature to drop so suddenly and greatly solely as a consequence of smoke visible AOD ramping up.” Indeed, this was a topic of much discussion among the authors of S24. However, no scientific analysis or justification was made by F25 to support this conclusion. Thus, we investigated the cooling rate of the surface due to shadowing alone using GOES-16 TIR BTs and ASOS 2-m air temperature measurements obtained during the total solar eclipse of 8 April 2024. A total solar eclipse provides a good case to study the observable impacts of strong, sudden surface shadowing on the surface skin temperature because the satellite can clearly see the shadowed surface. It is well documented that the atmosphere and Earth’s surface cool during total solar eclipses due to shadowing (Garreaud et al., 2023; Good, 2016; Kadygrov et al., 2013; Mahmood et al., 2020; Szałowski, 2002; Trees et al., 2024). We primarily analyzed data in the Missouri bootheel region of southeastern Missouri, though we also analyzed areas of Arkansas and Indiana. All three of these regions were in the path of totality of the 2024 total solar eclipse, so they experienced the strongest shadowing.

We analyzed GOES-16 data every half hour from 12:00 UTC until 16:00 UTC, then analyzed data every five minutes from 16:00 UTC until 21:00 UTC to cover the time of the eclipse, and then data every half hour from 21:00 UTC until 00:00 UTC on 9 April 2024. At each GOES-16 analysis time, we identified the maximum visible reflectance (red) and maximum TIR BT (black) from the boxed region in Fig. 18a and b. We conducted the regional analysis to avoid thermal contamination from cirrus clouds that moved through the domain and ensure the time series of TIR data represented the surface conditions. The time series of regional maximum GOES-16 visible reflectance is plotted in red in Fig. 18c, while the regional maximum GOES-16 TIR BT is plotted in black in Fig. 18c. We also analyzed the 2-m air temperature measurements taken at the Kennett, MO ASOS station (KTKX), with the location of KTKX shown in blue in Fig. 18b and in the time series plot. Note that a GIF of the GOES-16 data is included as a supplement. Just before the start of the eclipse, the maximum regional GOES-16 TIR BT was about 308 K. However, as the eclipse began and the amount of sunlight reaching the surface was reduced, the GOES-16 TIR BT decreased substantially. By the end of totality at 19:00 UTC, the maximum regional GOES-16 TIR BT had decreased to 291 K, a roughly 17 K drop in just one hour. As the moon’s shadow left and the sunlight returned, the maximum regional GOES-16 TIR BT increased very quickly, warming back up to about 304 K by 20:00 UTC, a roughly 13 K increase in one hour. While not shown, we also conducted similar analyses in the totality path in Arkansas and Indiana, finding cooling rates of 13 K per hour and 11 K per hour, respectively. These results clearly show that the surface skin temperature responds quickly to sudden and significant reductions in insolation at the surface. If a surface TIR cooling rate of 17 K per hour from shadowing alone was detected in April in southeastern Missouri, a relatively moist, temperate area of the country, we argue that a cooling

rate of 19 K per hour from shadowing alone is plausible in the dry and arid western United States in the summertime.

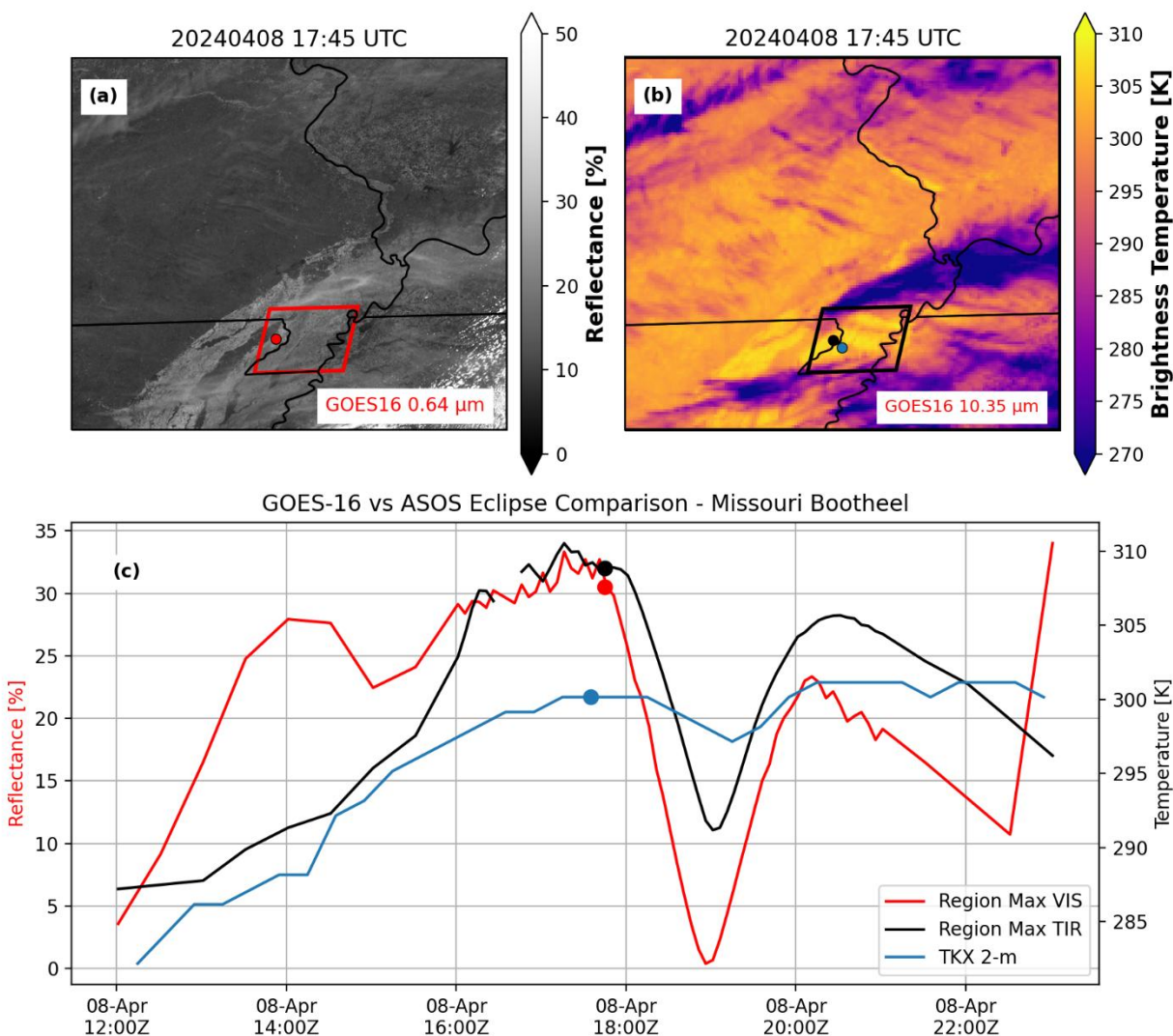


Figure 18. Top: GOES-16 (a) 0.64 μm reflectance and (b) 10.35 μm brightness temperature in southeastern Missouri just before the start of the 2024 total solar eclipse. Bottom: Time series of maximum regional GOES-16 0.64 μm reflectance (red), maximum regional GOES-16 10.35 μm brightness temperature (black), and KTKX ASOS 2-m air temperature (blue), with the GOES-16 analysis regions shown in the red and black boxes in panels (a) and (b), respectively.

5. Summary

In F25, the author argues that MODIS data alone cannot capture the changing emission scenarios of western US wildfires. It is true that Aqua MODIS provides only one set of observations during the daytime, but as our analyses in both the original paper and in this response show, MODIS data do prove sufficient to determine if large particles are widespread in smoke plumes at the time of the satellite overpass. Using the change in AOD with wavelength, and due to the overall lack of

smoke plume signatures in the SWIR wavelengths, we conclude that the smoke in the areas far downwind of the fire consisted of primarily fine-mode particles. Using similar methods, we can also determine when notable SWIR signals suggest that large particles were likely present in the plume. It is worth noting that similar analyses conducted using data from VIIRS and GOES-16/17 yielded similar results, and NEXRAD radar observations from the three nearest WSR-88D radars corroborate the analyses. While analyzing the smoke plume at other times from GOES is indeed useful and can help identify other sources of plume TIR cooling signals at other times, we showed that the multispectral MODIS data are sufficient for determining the likely sources of TIR cooling found in MODIS observations.

In F25, the author argues that the existence of nighttime TIR cooling signals on other days proves that the cooling was driven by ash or other large particles. We agree with F25 that there are cases in which flare-ups and pyroCb activity led to the generation of ash and other large particles that caused significant TIR cooling signals. This is clearly evident from both MODIS, GOES, and NEXRAD observations. However, this does not mean that all TIR cooling signals within smoke plumes are from large particles. We have clear evidence that there is observable TIR cooling in smoke plumes when large particles are not dominant. The interception of terrestrial longwave emission by lofted large particles and cooling of the surface from shadowing are two separate phenomena that can both be observed.

In F25, the author argues that the 2-m temperature measurements taken by O05 and the GOES-16 TIR brightness temperatures at the same location on 22 July 2021 do not agree, so GOES-16 must have been observing large particles over the ASOS site. We agree that the data do appear decoupled. However, we have several issues with the analysis presented in F25. The Chester, CA ASOS site (O05) is located less than 1 km away from the shore of Lake Almanor. The nadir footprint size of the GOES-16 TIR channel is 2 km, and towards the limb of the GOES-16 viewpoint, the footprint size is likely 3-4 km wide. The point-spread function in the GOES-16 footprint and geolocation errors are also unknown, so we cannot be certain that the surface of Lake Almanor was not contaminating the TIR data observed by GOES-16 at the latitude and longitude of the O05 ASOS site. This could explain why the GOES-16 data exhibited lower amplitude diurnal temperature variations than the 2-m air temperatures observed by the ASOS instrument. However, even if the GOES-16 BTs over O05 were detecting large particles, this does not mean that the TIR cooling observed hundreds of kilometers downwind of the fire was caused by large particles. The evidence in those regions points towards surface shadowing as the driver of the TIR cooling signal.

Our analysis of the smoke plume over Grand Forks, ND on 29 June 2015 showed that surface cooling beneath fine-mode smoke particles can indeed be detected by TIR channels on satellite-based sensors. Aqua MODIS true-color imagery showed dense smoke across the Northern Plains, along with strong TIR cooling in the smoky regions. AERONET observations from Grand Forks confirm that the smoke plume consisted entirely of fine-mode smoke particles, ruling out the

interception of terrestrial longwave emission by large particles as a cause of the observed TIR cooling. With previous work identifying strong cooling in near-surface air temperature measurements (Carson-Marquis et al., 2021; Zhang et al., 2016), and with MODIS TIR data showing cooling in similar areas, these results support the hypothesis of S24 that shadow-based surface cooling beneath dense plumes of fine-mode smoke particles can be detected by satellite-based TIR channels. The existence of light but non-negligible SWIR AOD observed by AERONET in this fine-mode plume shows that the presence of some SWIR signals alone does not prove the existence of coarse-mode particles in a smoke plume.

In F25, the author argues surface cooling rates of 19 K per hour from shadowing alone seem physically unreasonable due to Earth's thermal inertia. Our analysis of the 2024 total solar eclipse presented in this response shows such a cooling rate from shadowing is plausible. GOES-16 TIR BTs during the 2024 total solar eclipse exhibited cooling of 17 K within one hour in the Missouri bootheel region, with 13 K per hour of warming immediately after totality. With this strong of surface cooling observed in the relatively moist and temperate eastern United States, we argue that it is plausible for the surface to cool at 19 K per hour in the dry, hot, and arid western US, especially in conditions that preceded intense wildfire development.

The point of S24 was not to argue that all TIR cooling signals observed within smoke plumes are caused by surface shadowing. As presented in F25 and analyzed in this response, there certainly are cases in which ash and other large particles cause significant TIR cooling signals. However, this does not mean that all TIR cooling signals observed within smoke plumes are caused by large particles. As we showed in S24 and in this response, there are cases in which strong TIR cooling is observed within smoke plumes, but observational analyses show that the plumes in those areas consisted of primarily fine-mode smoke particles, not the coarse or large particles that would cause thermal signatures. The observational evidence supports multiple causes of TIR cooling signals in smoke plumes: interception of terrestrial longwave emission by large particles and cooling of the surface due to shadowing by fine-mode particles. Regardless of the source of the TIR cooling signals observed in multispectral data, CERES flux observations from each case analyzed in this response clearly show notable (and at times very strong) reductions in TOA LWF within smoke plumes, which supports the final conclusion of S24 that reductions in LWF in smoke plumes moderate the total TOA radiative impacts of smoke plumes and must be considered in future studies.

6. References

Carson-Marquis, B. N., Zhang, J., Xian, P., Reid, J. S., and Marquis, J. W.: Improving WRF-Chem Meteorological Analyses and Forecasts over Aerosol-Polluted Regions by Incorporating NAAPS Aerosol Analyses, *J. Appl. Meteorol. Climatol.*, 60, 839–855, <https://doi.org/10.1175/JAMC-D-20-0174.1>, 2021.

Garreaud, R., Bozkurt, D., Spangrude, C., Carrasco-Escaff, T., Rondanelli, R., Muñoz, R., Jubier, X. M., Lazzara, M., Keller, L., and Rojo, P.: Cooling the Coldest Continent: The 4 December 2021 Total Solar Eclipse over Antarctica, *Bull. Am. Meteorol. Soc.*, 104, E2265–E2285, <https://doi.org/10.1175/BAMS-D-22-0272.1>, 2023.

Good, E.: Satellite observations of surface temperature during the March 2015 total solar eclipse, *Philos. Trans. R. Soc. Math. Phys. Eng. Sci.*, 374, 20150219, <https://doi.org/10.1098/rsta.2015.0219>, 2016.

Hoekzema, N. M., Garcia-Comas, M., Stenzel, O. J., Grieger, B., Markiewicz, W. J., Gwinner, K., and Keller, H. U.: Optical depth and its scale-height in Valles Marineris from HRSC stereo images, *Earth Planet. Sci. Lett.*, 294, 534–540, <https://doi.org/10.1016/j.epsl.2010.02.009>, 2010.

Kadygrov, E. N., Miller, E. A., and Troitsky, A. V.: Study of Atmospheric Boundary Layer Thermodynamics During Total Solar Eclipses, *IEEE Trans. Geosci. Remote Sens.*, 51, 4672–4677, <https://doi.org/10.1109/TGRS.2013.2248014>, 2013.

Kaufman, Y. J., Tanré, D., Remer, L. A., Vermote, E. F., Chu, A., and Holben, B. N.: Operational remote sensing of tropospheric aerosol over land from EOS moderate resolution imaging spectroradiometer, *J. Geophys. Res. Atmospheres*, 102, 17051–17067, <https://doi.org/10.1029/96JD03988>, 1997.

Mahmood, R., Schargorodski, M., Rappin, E., Griffin, M., Collins, P., Knupp, K., Quilligan, A., Wade, R., and Cary, K.: The Total Solar Eclipse of 2017: Meteorological Observations from a Statewide Mesonet and Atmospheric Profiling Systems, *Bull. Am. Meteorol. Soc.*, 101, E720–E737, <https://doi.org/10.1175/BAMS-D-19-0051.1>, 2020.

McCarthy, N., Guyot, A., Dowdy, A., and McGowan, H.: Wildfire and Weather Radar: A Review, *J. Geophys. Res. Atmospheres*, 124, 266–286, <https://doi.org/10.1029/2018JD029285>, 2019.

Remer, L. A., Kaufman, Y. J., Tanré, D., Mattoo, S., Chu, D. A., Martins, J. V., Li, R.-R., Ichoku, C., Levy, R. C., Kleidman, R. G., Eck, T. F., Vermote, E., and Holben, B. N.: The MODIS Aerosol Algorithm, Products, and Validation, *J. Atmospheric Sci.*, 62, 947–973, <https://doi.org/10.1175/JAS3385.1>, 2005.

Rogers, R. R. and Brown, W. O. J.: Radar Observations of a Major Industrial Fire, *Bull. Am. Meteorol. Soc.*, 78, 803–814, [https://doi.org/10.1175/1520-0477\(1997\)078%253C0803:ROOAMI%253E2.0.CO;2](https://doi.org/10.1175/1520-0477(1997)078%253C0803:ROOAMI%253E2.0.CO;2), 1997.

Sorenson, B. T., Reid, J. S., Zhang, J., Holz, R. E., Smith Sr., W. L., and Gumber, A.: Thermal infrared observations of a western United States biomass burning aerosol plume, *Atmospheric Chem. Phys.*, 24, 1231–1248, <https://doi.org/10.5194/acp-24-1231-2024>, 2024.

Szałowski, K.: The effect of the solar eclipse on the air temperature near the ground, *J. Atmospheric Sol.-Terr. Phys.*, 64, 1589–1600, [https://doi.org/10.1016/S1364-6826\(02\)00134-7](https://doi.org/10.1016/S1364-6826(02)00134-7), 2002.

Thorpe, T. E.: A history of Mars atmospheric opacity in the Southern Hemisphere during the Viking extended mission, *J. Geophys. Res. Space Phys.*, 84, 6663–6683, <https://doi.org/10.1029/JA084iA11p06663>, 1979.

Trees, V. J. H., de Roode, S. R., Wiltink, J. I., Meirink, J. F., Wang, P., Stammes, P., and Siebesma, A. P.: Clouds dissipate quickly during solar eclipses as the land surface cools, *Commun. Earth Environ.*, 5, 71, <https://doi.org/10.1038/s43247-024-01213-0>, 2024.

Zhang, J., Reid, J. S., Christensen, M., and Benedetti, A.: An evaluation of the impact of aerosol particles on weather forecasts from a biomass burning aerosol event over the Midwestern United States: observational-based analysis of surface temperature, *Atmospheric Chem. Phys.*, 16, 6475–6494, <https://doi.org/10.5194/acp-16-6475-2016>, 2016.